

Spectral Function for the S=1 Heisenberg Antiferromagnetic Chain

Steven R. White

Department of Physics and Astronomy, University of California, Irvine CA 92697, USA

Ian Affleck

Department of Physics and Astronomy, University of British Columbia, Vancouver, British Columbia, Canada V6T 1Z1

(Dated: today)

We study the spectral function, $S(k, \omega)$ for the spin-1, one dimensional antiferromagnetic chain using a time-dependent density matrix renormalization group (DMRG) numerical method. We develop methods for extrapolating the time dependent correlation functions to larger times in order to enhance the frequency resolution. The resulting spectral functions are impressively precise and accurate. Our results confirm many qualitative expectations from non-linear σ model methods and test them quantitatively. The critical wave-vector at which the single particle excitation emerges from the 2-particle continuum is estimated to be $0.23\pi - 0.24\pi$.

I. INTRODUCTION

The $S = 1$ Heisenberg antiferromagnetic chain,

$$H = J \sum_j \vec{S}_j \cdot \vec{S}_{j+1}, \quad (1)$$

has been a subject of intense theoretical and experimental study since Haldane's observation that it has an excitation gap above a singlet ground state to a triplet excited state, quite unlike the $S=1/2$ case. Much has been learned about the time independent properties using a combination of analytic and numerical methods, in particular the density matrix renormalization group (DMRG).¹ Our knowledge of dynamical properties, while substantial, leaves more room for improvement.² Recently, DMRG has been significantly extended to allow direct calculation of time dependence (tDMRG)^{3,4,5,6} and time-dependent correlation functions in particular. In this paper we will utilize tDMRG to calculate high-resolution spectral functions for the $S = 1$ chain for a broad range of momenta. Some of the numerical techniques developed here were briefly described in Ref. 7.

The spectral function we shall focus on, in the isotropic case, is

$$S(k, \omega) = \sum_{j=-\infty}^{\infty} e^{-ikj} \int_{-\infty}^{\infty} dt e^{i\omega t} \langle 0 | S_j^a(t) S_0^a(0) | 0 \rangle \quad (2)$$

where $S(k, \omega) \equiv S^{aa}(k, \omega)$, with $a = x, y, \text{ or } z$, and the subscripts on S indicate sites. The tDMRG method calculates the space-time dependent expectation values appearing in Eq. (2) directly, and then one performs the Fourier transforms (FTs) in Eq. (2) to obtain $S(k, \omega)$. The crucial practical issue for this approach, which we discuss in detail in this paper, is dealing with the finite range of times available from a tDMRG simulation. We find that two different methods for extrapolation in time to increase the range of times used in the FTs are both very useful for increasing the frequency resolution.

Much insight into the model can be obtained from an approximate mapping, based on the large S limit, onto

the non-linear σ -model (NL σ M) with Lagrangian density:

$$\mathcal{L} = \frac{1}{2gv} [(\partial_t \vec{\phi})^2 - v^2 \partial_x \vec{\phi}^2], \quad (3)$$

where the lattice spin operators are represented as:

$$\vec{S}_j \approx \frac{1}{vg} \vec{\phi} \times \partial_t \vec{\phi} + (-1)^j s \vec{\phi}, \quad (4)$$

$\phi^2 = 1$, v is the spin velocity and $g \approx 2/s$ is the coupling constant. $\vec{\phi}$ is the antiferromagnetic order parameter and $\vec{l} \equiv (1/vg) \vec{\phi} \times \partial_t \vec{\phi}$ is the uniform magnetization density. This low energy representation is only valid for wave-vectors near 0 and π . This field theory is known to have a singlet ground state in one space dimension, with a gap, Δ , to a massive spin-triplet of excitations. There are no bound states or any other single particle excitations besides this triplet. This implies that a single particle (δ -function) peak should appear in $S(k, \omega)$ near $k = \pi$ at energy Δ but near $k \approx 0$ the lowest excitations are a 2-particle continuum starting at 2Δ . Interaction effects mix $\vec{\phi}$ with $(\vec{\phi})^3$ [but not $(\vec{\phi})^2$ by symmetry] so that the theory also predicts a 3-particle continuum at $k \approx \pi$ starting at 3Δ , a 4-particle continuum at $k \approx 0$, et cetera. Continuity between $k \approx 0$ and $k \approx \pi$ then implies a qualitative sketch like Fig. 1 for the region of non-zero spectral weight. In particular, the single particle peak must emerge out of the 2-particle continuum at some critical wave-vector k_c . Integrability of the NL σ M allows for the calculation of exact form factors and hence predictions for the detailed shape of the 2-particle contribution to $S(k, \omega)$ near $k \approx 0$ and the 3-particle contribution near $k \approx \pi$.^{11,12}

Since the field theory is based on $S \rightarrow \infty$ and is only valid for k very close to 0 and π it is unclear how well any of these predictions should describe the $S=1$ case. Various comparisons of NL σ M predictions with numerical results have been performed before, but these have necessarily focused primarily on equal time correlators and thermodynamic quantities. Experiments on quasi-1-dimensional antiferromagnets have clearly confirmed the

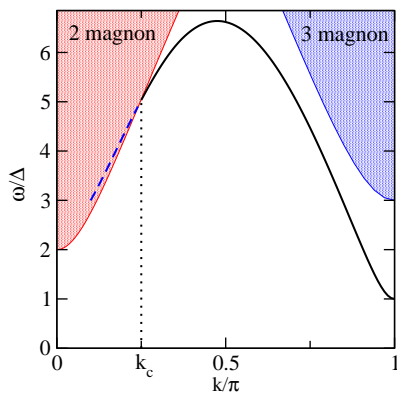


FIG. 1: General features of the spectral function. The four and higher magnon continua are not shown.

Haldane gap but the 2-particle nature of the small k excitations and the existence of a gap at $k = \pi$ from the single particle excitation at Δ to the bottom of the 3-particle continuum at 3Δ have not been confirmed and have led to some questioning of the validity of these field theory predictions.

One of the purposes of this paper is to compare our tDMRG calculations of $S(k, \omega)$ with the NL σ M predictions. In addition, we will determine k_c and examine the behavior near this wave-vector.

In Sec. II we review the time dependent DMRG algorithm and discuss methods for extrapolating the time-dependent correlation function to longer times before Fourier transforming. In Sec. III we discuss properties of the single magnon excitation. In Sec. IV we discuss S near $k \approx 0$ and compare with the 2-magnon NL σ M predictions. In Sec. V we study S near $k \approx \pi$ and compare with the 1-magnon plus 3-magnons predictions. In Sec. VI we study intermediate k in the vicinity of k_c where the single magnon peak first emerges. Sec. VII contains our conclusions.

II. TIME DEPENDENT DMRG AND EXTRAPOLATION IN TIME

The time dependent DMRG method^{3,4,5} has been described elsewhere; here we describe some of the practical issues related to obtaining dynamical spectra. First, we describe the specific tDMRG algorithms used; second, time step and truncation errors; and third, extrapolation in time and windowing for time Fourier transforms.

The first step of a calculation is to use ordinary DMRG to find the ground state of a finite open system to high accuracy, with typical lengths being $L = 200 - 400$. To avoid $S = 1/2$ end states, we put real $S = 1/2$ spins on the first and last sites. Let i be one of the two center sites. After obtaining the ground state ϕ , we apply the operator S_i^+ or S_i^z to create a state which is a mixture of excited states, $\psi(t = 0)$. We target and time evolve

ψ , and also, in order to minimize time step errors in correlation functions, ϕ . As the time evolution occurs, we measure the correlation function $S(j - i, t)$ when the tDMRG step is at site j , accumulating the function for a wide range of separations and times.⁴

For the time evolution we use only the Suzuki-Trotter decomposition methods, which are very efficient for chain systems with only nearest neighbor interactions. We use two different variations. First, we use the original method of White and Feiguin,⁴ which has second order Trotter errors. An advantage of this method is that every DMRG step has a time evolution bond operator applied, whereas Trotter methods splitting the links into even and odd groups⁵ apply a time evolution operator on only half the steps of a sweep, resulting in roughly twice as much total truncation error per unit time evolved. To obtain a measurement for a specific time, we perform the measurements in a half sweep without any time evolution. Thus, including measurements, we evolve in the repeated 6 half-sweep pattern: evolve left-to-right, evolve right-to-left, left-to-right measurement half-sweep (without time evolution), evolve right-to-left, evolve left-to-right, right-to-left measurement half-sweep. During each half-sweep time evolution step, we evolve a time step τ , so that measurements are available with a time step of 2τ . Typically we use $\tau = 0.1$. (We set $J = 1$.)

The second method we use is a fourth order Trotter method,^{6,8} which with $\tau = 0.1$ virtually eliminates time-step errors, at the expense of more sweeps for a given time, and consequently larger accumulated truncation error. We show below that the *second order* Trotter errors from the first method with a time step of $\tau = 0.1$ primarily lead to modest frequency shifts, shifting the Haldane gap by about 1%, for example. (The rate of decay in time of the correlation functions seems not to be strongly effected.) For high accuracy studies it is more efficient to use the fourth order method rather than simply reducing τ . The decomposition we use is⁸

$$e^{(A+B)\tau + \mathcal{O}(\tau^5)} = e^{A\theta\frac{\tau}{2}} e^{B\theta\tau} e^{A(1-\theta)\frac{\tau}{2}} e^{B(1-2\theta)\tau} \times e^{A(1-\theta)\frac{\tau}{2}} e^{B\theta\tau} e^{A\theta\frac{\tau}{2}} \quad (5)$$

with $\theta = 1/(2 - 2^{1/3}) \approx 1.35$. Here A would represent, say, the odd bonds, and B the even, and each of the seven terms is applied in a half-sweep. Adding to this a measurement half-sweep, a total of eight half-sweeps are needed to evolve by τ , with measurements available with a time step of τ .

Generally we specify a desired truncation error for each step, and vary the number of states kept m to achieve this truncation error. However, we also constrain m to be no larger than a specified m_{limit} (typically 1000-2000), and no smaller than a minimum m_{min} (typically 100-150). The purpose of m_{min} is to reduce the truncation error to near zero, at little cost, in steps where the state has very small entanglement. (These small entanglement steps occur outside the “light cone” of the initial disturbance at site i , and time 0.) We specify a m_{limit} to avoid memory

limitations and to avoid a handful of steps (near site i) taking a large fraction of the computer time.

The total accumulated truncation error, ε_{tot} , summed over all DMRG steps since the start of the time evolution, is readily available and useful. At each step, a small part of each wavefunction is discarded; the truncation error is the magnitude squared of these small parts. In Fig. 2 we show that ε_{tot} gives a rough estimate of the typical errors to be expected in measurements at that time. The plot compares ε_{tot} with the errors in $S(x, t)$ for $x = j - i = 0$ and $x = 1$. The errors in $S(x, t)$ were estimated by running with two different truncation error parameters ε , $\varepsilon = 2 \times 10^{-10}$ and $\varepsilon = 4 \times 10^{-10}$. We also see that errors of order 10^{-5} are computationally feasible for times $t < 10$, but that the errors steadily grow with time. In this case the errors grow roughly linearly with time because a target truncation error per step was specified, with the upper limit m_{limit} playing a small role.

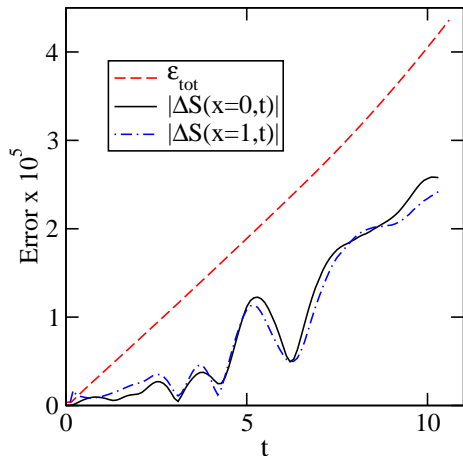


FIG. 2: Comparison of the errors in measurements of $S(x, t)$ and the total accumulated truncation error ε_{tot} . Two runs were made using the 4th order Trotter decomposition, both with $\tau = 0.1$, with $\varepsilon = 2 \times 10^{-10}$ and $\varepsilon = 4 \times 10^{-10}$. The values of ΔS were the difference in the results between these two runs. The value for ε_{tot} was for the larger ε run.

To clarify further how this works in Fig. 3 we compare two runs, one a second order Trotter method, the other the more accurate run of Fig. 2. Both runs took comparable amounts of computer time. We define m_{max} to be the maximum number of states kept over all the steps in a half-sweep. Clearly $m_{\text{max}} \leq m_{\text{limit}}$. In each half-sweep, the largest values of m were for steps near the center of the system, where the spin operator was applied. After a moderate time, for these steps near the center m was limited by m_{limit} . The relatively small number of these steps made the effect of m_{limit} on ε_{tot} small. The calculation time for a step is proportional to m^3 , so limiting m is important for efficiency.

The tDMRG yields directly the space-time dependent correlation function directly. The signal initiated by the

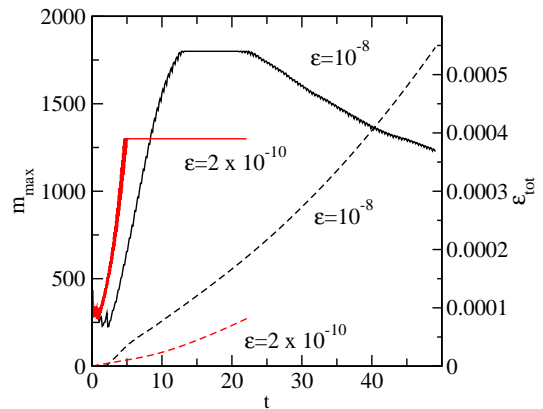


FIG. 3: Maximum number of states kept m_{max} versus time (upper-left curves), and total discarded weight ε_{tot} versus time (lower right curves) for the systems of Fig. 5. The simulation adjusted m at each step to try to achieve a total discarded weight of ε for that step, subject to a maximum m of either 1300 or 1800 (flat portions). The figure shows that in this case ε_{tot} depends more strongly on ε than on the maximum allowed m .

application of the spin operator in the center of the system spreads out with time. Because the system has a finite correlation length, the correlation function is only non negligible within a range of about $|vt|$ of the center, where v is the maximum spin velocity. We always keep the maximum time t_{max} of the simulation small enough so that the signal has not reached the edges at the end of the simulation. Hence there are essentially no spatial finite size effects. One can spatially Fourier transform (FT) $x \rightarrow k$ for any k ; the available values of k are continuous, not discrete. On the other hand, the feasible t_{max} is strictly limited by the available computer time, and the correlation functions decay slowly or not at all in time. Truncation of the signal following by an FT $t \rightarrow \omega$ would result in severe “ringing”. The standard approach is to multiply the signal by a windowing function, which typically resembles a Gaussian centered at $t = 0$ but which vanishes exactly at $\pm t_{\text{max}}$. A drawback of this approach is that most of the data gets “thrown away”, and the frequency broadening of the spectrum is large.

To avoid this over-broadening, we have developed an alternative approach based on linear prediction.⁹ Before the time-frequency FT, we extrapolate the time signal to long times using linear prediction. We then apply a broad window which does not throw away a significant amount of the original data. Linear prediction extrapolates a discrete equally spaced time series $\{y_i\}$ as

$$y_i = \sum_{j=1}^n d_j y_{i-j} \quad (6)$$

The coefficients d_j are determined by the known data points $\{y_i\}$ by requiring that their prediction for each

point y_i , based on $y_{i-n} \dots y_{i-1}$, vary as little as possible from the actual value y_i , using a least-squares criterion. One finds that the d_j are determined from correlation functions $\langle y_i y_{i+j} \rangle$, where the average is over i , and the principle computational work in determining d_j is the inverse of a $n \times n$ matrix. In our work we have used $n = 20$, so that the numerical work involved in the extrapolation is negligible.

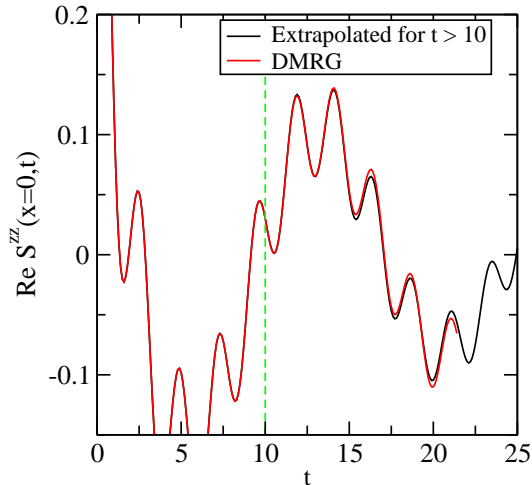


FIG. 4: DMRG results for the real part of the onsite spin-spin correlation function $S^{zz}(x=0, t)$ for the more accurate run of Fig. 2. The red curve represents DMRG data out to $t = 22$; the black curve is the DMRG data for $t \leq 10$ and a linear extrapolation for $t > 10$.

In Fig. 4 we show the effectiveness of this extrapolation. For this run which had $t_{\max} = 22$, the data for $t \leq 10$ was extrapolated to longer times and compared with the DMRG results. The error in the extrapolation starts out small and grows reasonable slowly. Provided one does not rely on too long an extrapolation to try to achieve higher frequency resolution than the data supports, this method performs much better than ordinary windowing methods.

In Fig. 5 we compare the density of states, defined as $N(\omega) = S^{zz}(x=0, \omega)$, for the two systems of Fig. 3. After the linear extrapolation, the results were multiplied by a Gaussian window $\exp[-t^2/(20t_{\max}^2)]$ before Fourier transforming. On this scale the effects of the Trotter errors in the 2nd order data are almost not visible. The results are considerably sharper than with the alternative method which did not use extrapolation. The sharp peaks are broadened square root singularities from the top and the bottom of the single-magnon dispersion. Above the top of the band, two- and three-magnon contributions to the spectrum are visible in a small tail. Using a larger window width would increase the resolution at the cost of increasing the likelihood of artifacts from the extrapolation. We will consistently use this window width. Assuming the extrapolation is accurate, this means that our spectra should look like the exact spectra,

but broadened by convolving with a gaussian

$$\exp(-\frac{1}{2}\omega^2/W^2) \quad (7)$$

where the frequency resolution is $W = (t_{\max}\sqrt{10})^{-1}$.

Another approach is to fit the moderate time data to the correct asymptotic long-time form, in this case stemming from the square root singularities, to extrapolate to long times very accurately. The linear extrapolation asymptotically gives exponential decays in time, an incorrect assumption in this case, so for very long times the fitting method can be more accurate. A disadvantage of the fitting method is that it assumes one has some understanding of the results analytically. Another disadvantage is that the fitting process can take much more computer time than the linear prediction method, although still much less than tDMRG simulation itself. In cases where one does not know what sort of spectra to expect, one can first fit with the linear prediction method, and then guess an asymptotic form for fitting.

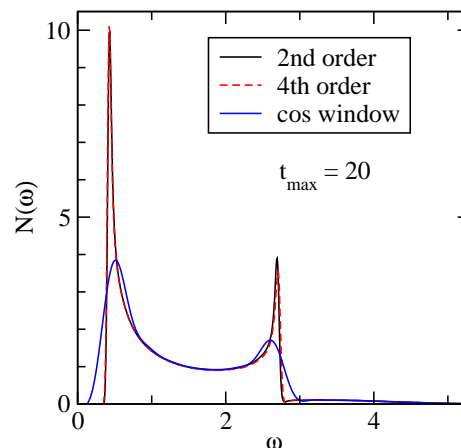


FIG. 5: Results for the density of states $N(\omega)$ for the two systems of Fig. 3, with linear extrapolation utilizing only the data out to $t_{\max} = 20$. The two curves are almost identical. The third curve used the 2nd order data but did not utilize extrapolation; instead, the data out to t_{\max} was multiplied by a simple finite window based on the cosine function.

For the case of $N(\omega)$, we have leading singularities of the form

$$a\theta(\omega - \Delta)(\omega - \Delta)^{-1/2} + b\theta(\Omega - \omega)(\Omega - \omega)^{-1/2} \quad (8)$$

where Ω is the maximum in the single magnon dispersion relation near $\pi/2$ of about 2.725. This Fourier transforms to long time tails with leading terms of the form

$$A \exp(-i\Delta t)t^{-1/2} + B \exp(-i\Omega t)t^{-1/2}. \quad (9)$$

A more convenient form for fitting comes from the Fourier transform integral identities

$$\begin{aligned} \int_{-\infty}^{\infty} d\omega e^{-i\omega t} \theta(\omega - b)e^{-a(\omega - b)}(\omega - b)^g \\ = \Gamma(1 + g)e^{-ibt}(a + it)^{-1-g} \end{aligned} \quad (10)$$

and

$$\int_{-\infty}^{\infty} d\omega e^{-i\omega t} \theta(b-\omega) e^{-a(b-\omega)} (b-\omega)^g = \Gamma(1+g) e^{-ibt} (a-it)^{-1-g}. \quad (11)$$

These identities are useful because the frequency expressions have only a single one-sided singularity, and convenient well-behaved Fourier transforms. Eq. (10) is useful for describing a singularity on a lower edge, while Eq. (11) describes an upper edge. Thus to fit to the tDMRG data for the Fourier transform of $N(\omega)$, we use the asymptotic form

$$A \exp(-i\Delta t) (a+it)^{-1/2} + B \exp(-i\Omega t) (b-it)^{-1/2}. \quad (12)$$

Fitting the accurate 4th order data over the time range 10 – 20 with this form, we find that the fit within this range matches the data very accurately, with a typical absolute deviation of about 2×10^{-4} , or a relative error of about 10^{-3} .

Using the fitting parameters and asymptotic form, one extends the data to large times. We did not use the identities Eqs. (10) and (11) to help perform the Fourier transform (although this might be convenient); we simply used a fast Fourier transform over a very large range of times (e.g. $-10000 \leq t \leq 10000$). Over the fitting region in time a smooth transition is made from the data for small times to the fit for large times. The results of this procedure for $N(\omega)$ are shown in Fig. 6. The fits allowed both Δ and Ω to vary; the result for the gap for the time range 10 – 20 was $\Delta = 0.4104327$, accurate to 4 digits (see next section). The resulting spectra, based on fitting over different time ranges, appears to be accurate to the line width in the figure.

III. SINGLE MAGNON RESULTS

Fourier transforming the DMRG $S(x, t)$ data $x \rightarrow k$, we obtain $S(k, t)$ for any k . The time Fourier transform gives spectra with (potentially) single magnon and multimagnon contributions. As we discuss below, for $k_c < k < \pi$, with $k_c \approx 0.23\pi - 0.24\pi$, a single magnon delta function peak is present, plus multimagnon continua at higher frequencies. In this section we focus on this well-defined single-magnon mode.

First consider the band minimum, at $k = \pi$, where the excitation energy is the Haldane gap. The most accurate method to determine the Haldane gap is still ground state DMRG, where we have used the same method as in Ref. 10, but with up to $m = 500$ and $L = 400$, to determine the Haldane gap to very high accuracy, $\Delta = 0.41047925(4)$. (The end coupling used to make the lowest excitation have $k = \pm\pi$ was $J_{\text{end}} = 0.50865$, compared to 0.5088 in Ref. 10.)

In Fig. 7, we show results for $S(\pi, \omega)$ near $\omega = \Delta$. Linear extrapolation plus Fourier transforming as described above give rather narrow Gaussian-shaped peaks. The

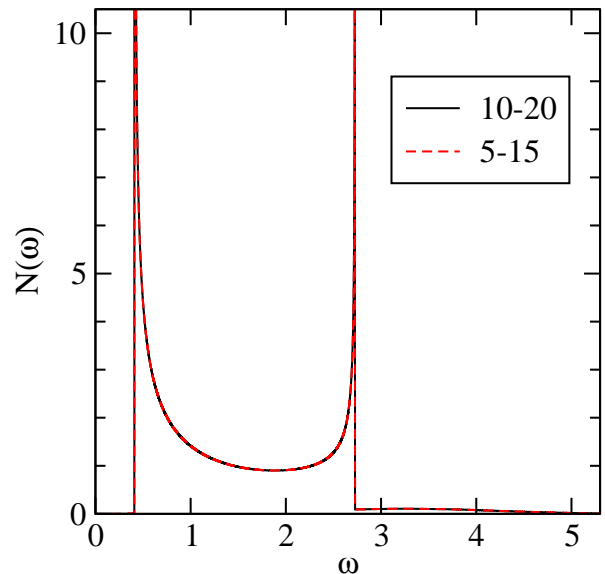


FIG. 6: Results for the density of states $N(\omega)$ from fitting to the asymptotic form Eq. (12) over the time range indicated in the caption, and then extending to very large times with the fit before Fourier transforming. The two curves overlap, indicating that the error in the determination of $N(\omega)$ is less than the line width.

2nd order peak is narrower because of a larger t_{max} , and it is shifted from the exact result because of Trotter error. Because two and three magnon contributions are very weak and separated in frequency from Δ , a least squares fit to a pure exponential is almost identical to the maximum of the broadened peaks. In fact, neglecting any Trotter shifts, either the maximum or the fit frequency provide much more accurate determinations of the exact magnon energy than the peak widths would indicate. For a set of k 's spaced 0.01π apart we have fit the time data either to a pure complex exponential (for $k > 1$) and for $k_c < k < 1$ to a complex exponential plus an asymptotic form describing the near-by two-magnon edge. These latter more complicated fits are discussed in Section VI. The frequency of the exponential term determines the dispersion $\varepsilon(k)$ for $k > k_c$. With this fitting approach, a larger t_{max} is not very important compared to the Trotter error, so we utilize the 4th order data. The corresponding result for $\varepsilon(\pi)$ is 0.41050; the error is only a few times 10^{-5} . For smaller k the error is expected to be larger because the multimagnon continuum is larger relative to the single magnon peak, and the continuum is closer in frequency, but the errors for $k > k_c$ are probably no bigger than 10^{-3} .

In Fig. 8 we show $\varepsilon(k)$ from the 4th order run, along with an analytic fit motivated by the NL σ model. The massive triplet excitations of the NL σ M have the relativistic dispersion relation:

$$\epsilon_0(\tilde{k}) = \sqrt{\Delta^2 + v^2 \tilde{k}^2}. \quad (13)$$

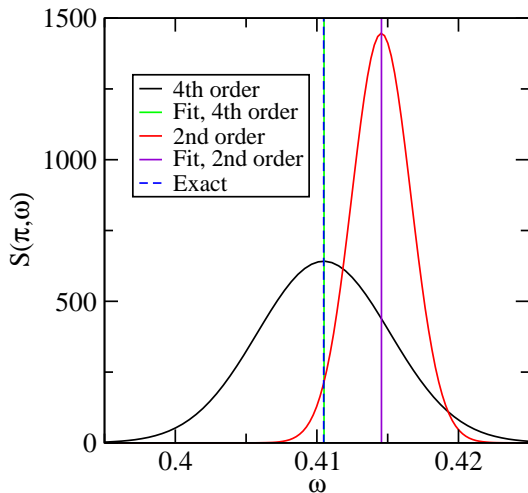


FIG. 7: Results for $S(\pi, \omega)$ for the two systems of Fig. 3. The Gaussian shaped curves come from linear extrapolation and Fourier transforming. The vertical lines represent delta functions coming from a least squares fit of $Ae^{i\omega t}$ to $S(\pi, t)$. The 4th order fit frequency and the “exact” ground state DMRG result are indistinguishable in this plot.

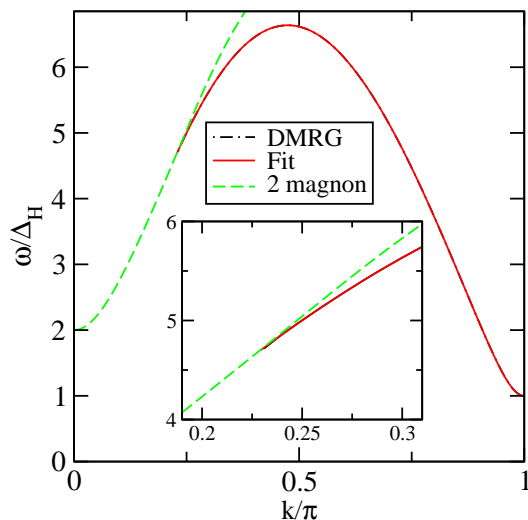


FIG. 8: Single magnon dispersion. The curve labeled “DMRG” comes from the fit of a pure exponential to the DMRG $S(k, t)$ data. The curve labeled “Fit” is the analytic expression Eq. (14). The final curve is the two magnon band minimum at $2\epsilon(\pi - k/2)$. The inset shows the region near k_c , where the magnon line enters the two magnon continuum. The first two curves are not very meaningful well below k_c , since there is no single magnon delta function.

Here the momentum \tilde{k} of the NL σ M is $k - \pi$ for the spin chain. In the NL σ M, \tilde{k} can take any real value. Of course, in the spin chain, crystal momenta lie in the Brillouin zone, $|k| < \pi$. This discrepancy limits the validity of the NL σ M, especially when we consider multi-particle excitations. $\epsilon_0(\tilde{k})$ is only an approximation to the exact

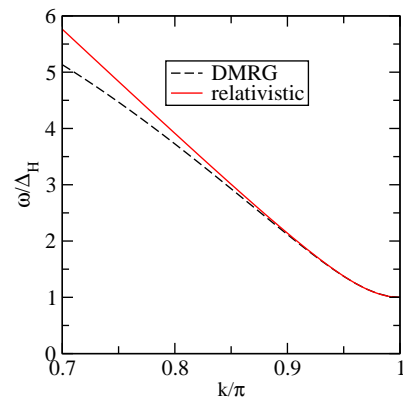


FIG. 9: Comparison of the single magnon dispersion from DMRG and the relativistic approximation, Eq. 13.

single magnon dispersion relation, $\epsilon(\tilde{k})$. We expect a perfectly stable single magnon excitation to exist for $\tilde{k} < \pi - k_c$ with this dispersion relation. Strictly speaking $\epsilon(\tilde{k})$ is not defined for $\tilde{k} > \pi - k_c$. The “Fit” curve shown in Fig. 8 is based on the expression

$$\epsilon(k) \approx \Delta \sqrt{1 + \sum_{n=1}^5 a_n \{1 - \cos[n(\pi - k)]\}}. \quad (14)$$

with the parameters a_n given in Table 1. The gap, at $k = \pi$, from the data used in the fit is $\Delta = 0.410504$; one could also use the more accurate value $\Delta = 0.41047925$. $\epsilon(k)$ goes through a maximum of 2.72551 at $k \approx .476\pi$ and has the value 1.96 at $k \approx 0.23\pi$ near where the single magnon excitation becomes unstable. There is an inflection point ($d^2\epsilon/dk^2 = 0$) at $k_{\text{in}} \approx 0.868\pi$. As shown in Fig. 9 $\epsilon(\tilde{k})$, agrees quite well with the Lorentz invariant approximation, $\epsilon_0(\tilde{k})$, for $\tilde{k} < 0.1\pi$, and reasonably well for $\tilde{k} < 0.2\pi$, with $v \approx 2.472$. Also shown in Fig. 8 is the two magnon band minimum, which for $|k| < 2(\pi - k_{\text{in}}) \approx 0.265\pi$ is given by $2\epsilon(\pi - k/2)$. Near $\tilde{k} \approx 0$, this is approximately

$$\epsilon(\tilde{k}) \rightarrow \Delta + \frac{(v\tilde{k})^2}{2\Delta}. \quad (15)$$

The intersection of the two magnon minimum and the single magnon dispersion line determines k_c , as show in the inset of Fig. 8.

The single magnon dispersion can be used to construct the multimagnon band minima and maxima, assuming that the magnon-magnon interactions are negligible, and adding the single magnon energies. The resulting bands are shown in Fig. 10. In this construction, it was assumed that the single magnon line stops abruptly at $0.23\pi \approx k_c$. This resulted in slope discontinuities visible in the two magnon band. However, at k_c , as we discuss below, the sharp “single magnon peak” can be described as either a single magnon or two magnon feature.

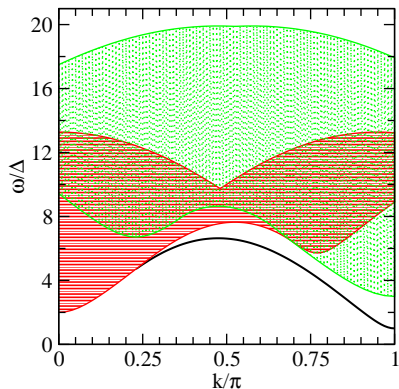


FIG. 10: Single magnon line (black solid line), two magnon band (horizontal line fill, red), and three magnon (dotted fill, green) bands.

This ambiguity effectively blurs the distinction between the two and three magnon bands near the slope discontinuities. If one changed the construction to include the broadened “single magnon peak” to values of k below k_c , the two magnon bandwidth would be broadened near the slope discontinuities. This suggests that, for example, at $k = \pi$ one might expect to see the two magnon band maximum as a visible feature of the spectrum, but one might not see anything for the two magnon minimum. (The spectrum at $k = \pi$ is shown in Section V.)

The amplitude of the single magnon peak is approximated well by¹¹

$$S(q, t = 0) \approx \frac{vZ}{\sqrt{v^2k^2 + \Delta^2}} \quad (16)$$

with $Z = 1.26$. A related quantity is the fraction of the spectral weight in the multimagnon continua, given by

$$f = \frac{S(q, t = 0) - A}{S(q, t = 0)} \quad (17)$$

where A is the amplitude of the single magnon peak. This quantity is shown in Fig. 11. It is interesting that f shows non monotonic behavior with k , with minima near $k = \pi/2$ and $k = \pi$. This non monotonic behavior is roughly correlated with the gap between the single magnon line and the lowest multi-magnon band mini-

TABLE I: Coefficients in the fit of the single magnon dispersion relation, Eq. (14).

n	a_n
1	1.96615
2	21.20162
3	-1.61279
4	-0.04766
5	0.02407

mum. Naively, one might expect that a nearby continuum has an easier time than a faraway one does in taking spectral weight from the single magnon line.

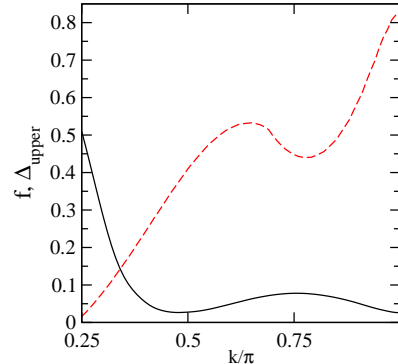


FIG. 11: Fraction of the spectral weight in the multimagnon continua for $k > k_c$, shown by the solid black line. The gap between the single magnon line and the lowest multimagnon band is shown by the dashed red line.

IV. $k \approx 0$

We now discuss the properties of the spectral function for small k . That $S \propto k^2$ as $k \rightarrow 0$ can easily be proven to be exactly true using the fact that $\sum_j S_j^z |0\rangle = 0$ (singlet ground state) and Taylor expanding $S(k, \omega)$ in Eq. (2) to second order in k . On general symmetry grounds, based on the NL σ M, we expect that near $k \approx 0$, S will contain only multi-particle continua corresponding to even numbers of bosons. At a finite small k , the lowest energy 2-magnon state with total momentum k is one in which each magnon has momentum $\pi + k/2$. Therefore, since the dispersion is even about π , the bottom of the 2-magnon continuum should be exactly at $2\epsilon(\pi - k/2)$. This remains true up to $k = 2(\pi - k_{\text{in}}) \approx .265\pi$ (recall $k_{\text{in}} \approx 0.868\pi$ is the inflection point). For a range of energies, at small enough k , the *only* possible excitations have 2 magnons. This is true up to $\omega = 4\epsilon(k/4)$, for $k < (\pi - k_{\text{in}})$.

A simplified, “mean field” version of the NL σ M is a free massive boson model with Lagrangian:

$$\mathcal{L} = \frac{1}{2v} [(\partial_t \vec{\phi})^2 - v^2 (\partial_x \vec{\phi})^2 - \Delta^2 (\vec{\phi})^2], \quad (18)$$

and no constraint on $\vec{\phi}$. Expanding $\vec{\phi}$ in boson creation and annihilation operators one finds the free boson result

$$S_0(k, \omega) \approx \frac{k^2 \sqrt{\omega^2 - (kv)^2 - 4\Delta^2}}{v[\omega^2 - (kv)^2]^{3/2}} \theta(\omega^2 - (vk)^2 - 4\Delta^2). \quad (19)$$

As expected from general principles, this vanishes quadratically as $k \rightarrow 0$, and also vanishes below the 2-magnon threshold, $\omega_{\text{th}} = 2\sqrt{\Delta^2 + (vk/2)^2}$. The exact

2-magnon expression for $S(k, \omega)$, in the NL σ M is known exactly and can be written:

$$S_{0\sigma}(k, \omega) = S_0(k, \omega) \frac{\pi^4}{64} \frac{1 + (\theta/\pi)^2}{1 + (\theta/2\pi)^2} \left(\frac{\tanh \theta/2}{\theta/2} \right)^2, \quad (20)$$

where the rapidity, θ , is defined by:

$$\theta = 2 \cosh^{-1}[(\omega^2 - v^2 k^2)/(4\Delta^2)]. \quad (21)$$

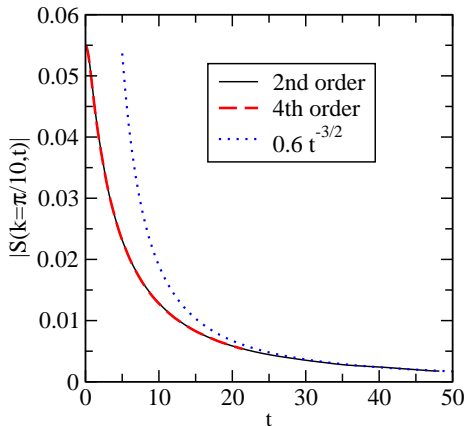


FIG. 12: Comparison of $|S(k, t)|$ for $k = \pi/10$ for two different runs, with 2nd order and 4th order Trotter decomposition runs of Fig. 2, and the asymptotic form expected analytically.

Just above ω_{th} , both Eqs. (19) and (20) rise as $(\omega - \omega_{\text{th}})^{1/2}$, which would lead to the asymptotic time behavior

$$S(k, t) \sim e^{-i\omega_{\text{th}}t} t^{-3/2}. \quad (22)$$

In Fig. 12 we compare $|S(k, t)|$ for a typical small value of k with $At^{-3/2}$, finding good agreement for large t with the empirical parameter $A = 0.6$. Using the linear prediction method, we Fourier transformed the $S(k, t)$ DMRG results for both runs, and in Fig. 13, they are compared to Eqs. (19) and (20). They look qualitatively similar. In particular, the threshold singularity appears the same and they have peaks at similar frequencies. However, the peak is about a factor of 2 larger in the DMRG data than in the NL σ M. Furthermore, the field theory results drop off much more slowly at large ω . This latter feature is to be expected since magnons of arbitrarily high momentum are included in the field theory while there is a cut off at the Brillouin zone boundary in reality.

A simple way to improve the high frequency behavior in the free boson approximation is to replace the relativistic model of Eq. (18), by a Hamiltonian:

$$H = \frac{1}{2} \sum_k [\vec{\Pi}_k \cdot \vec{\Pi}_{-k} + \epsilon^2(k) \vec{\phi}_k \cdot \vec{\phi}_{-k}], \quad (23)$$

where Π_k^a is canonically conjugate to ϕ_k^a and $\epsilon(k)$ is the

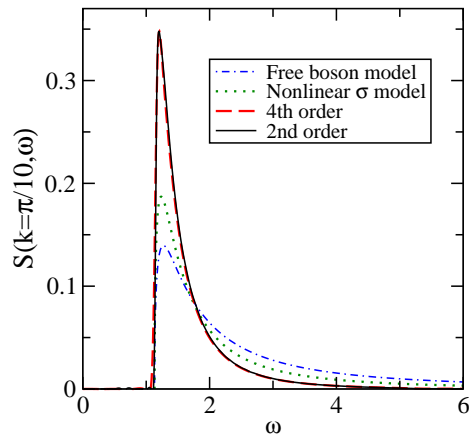


FIG. 13: $S(k, \omega)$ for $k = \pi/10$ for two different runs, with different accuracies and different total times, both Fourier transformed using linear extrapolation. For comparison, two analytic results, based on Eqs. (19) and (20), are shown.

numerically determined single magnon dispersion relation. The appropriate form of the small k spin operators:

$$\vec{S}_k \approx \sum_{k'} \vec{\phi}_{k'} \times \vec{\Pi}_{k-k'}, \quad (24)$$

is determined by the requirement that the spin commutation relations are obeyed and that \vec{S}_0 commute with the Hamiltonian. This changes $S_0(k, \omega)$ to:

$$S_0 \rightarrow \frac{[\epsilon(k') - \epsilon(k - k')]^2}{2\epsilon(k')\epsilon(k - k')|\epsilon'(k') - \epsilon'(k - k')|}, \quad (25)$$

where $\epsilon(k)$ is the exact (numerically determined) dispersion relation and $\epsilon'(k)$ denotes its derivative. k' , the momentum of one of the 2 magnons, is determined from ω and k by energy-momentum conservation:

$$\epsilon(k') + \epsilon(k - k') = \omega. \quad (26)$$

For low enough energy, there is only one pair of solutions to Eq. (26), and one element of the pair should be chosen in evaluating Eq. (25). The resulting improvement of the free boson result is shown in Fig. 14. As expected, there is little change near the peak and threshold, but the high energy tail is cut off. (Here we restricted each boson to have $|\tilde{k}| < \pi/2$.)

V. $k \approx \pi$

In addition to the single magnon mode, which has most of the spectral weight near $k = \pi$ there is also a contribution from 3, 5, ... magnons. Of these, the largest is expected to be the 3-magnon contribution. The lower threshold for this, corresponding to each magnon having momentum $\tilde{k}/3$ is at $3\epsilon(\tilde{k}/3) \approx 3\sqrt{\Delta^2 + (v\tilde{k}/3)^2}$.

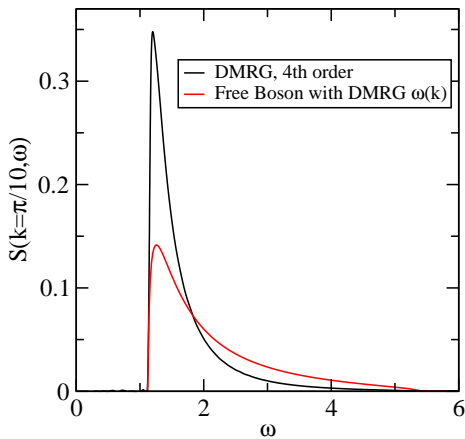


FIG. 14: $S(k, \omega)$ for $k = \pi/10$, comparing the near-exact DMRG results with the modified free boson result.

At small \tilde{k} the exact lower threshold approaches $3\Delta + (v\tilde{k})^2/(6\Delta)$. Note that the presence of a multi-magnon contribution is a consequence of inter-magnon interactions; it vanishes for the non-interacting model of Eq. (18). The exact 3-magnon form factor is known for the NL σ M and the resulting 3-magnon contribution to S can be expressed in terms of an elementary integral. The result is compared to our DMRG results in Fig. 15. Again there is a qualitative similarity, with a peak at a similar energy, but now the NL σ M peak is about 3 times too low and there is far too much spectral weight at high energies. The total spectral weight in the 3-magnon peak compared to that in the single magnon is found from DMRG to be 2.7%. The lower edge of the multimagnon band is given by the three magnon edge, c.f. Fig. 10. The band has a sharp dropoff at the two magnon band maximum. The three magnon band above that is rather small. As discussed earlier, one does not expect a sharp feature for the two magnon minimum (nominally near $\omega/\Delta \approx 9$), and none is visible.

VI. $k \approx k_c$

A remarkable feature of $S(k, \omega)$ which is completely missed by the NL σ M approach is the merging of the single particle peak into the 2-particle continuum at $k = k_c \approx 0.23\pi - 0.24\pi$. Results for $S(k, \omega)$ from the linear prediction method near k_c are shown in Fig. 16. Above k_c , one sees the separate single magnon peak, broadened by the finite run time and Fourier transform. By $k = 0.2\pi$ the peak has disappeared, and one sees a characteristic small k line shape. Close to k_c the broadening from the finite maximum time obscures the details of the spectrum.

The fitting method is very useful to capture the behavior of $S(k, \omega)$ near k_c more accurately. Just above k_c we expect a combination of a single magnon δ function peak

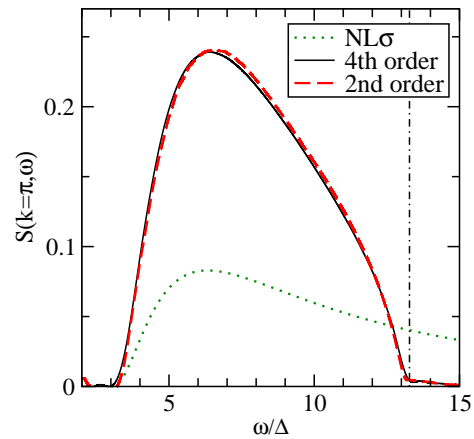


FIG. 15: $S(k, \omega)$ for $k = \pi$ in the multimagnon frequency regime for two different runs. Also shown are the results from the NL σ M model. The vertical line near $\omega/\Delta \approx 13$ is two times the maximum of the single magnon dispersion, roughly locating the top of the two magnon band. The tiny bump near $\omega/\Delta = 2$ is an artifact of the FT of the much larger single magnon peak at $\omega/\Delta = 1$, while we believe the small tail above $\omega/\Delta \approx 13$ is real.

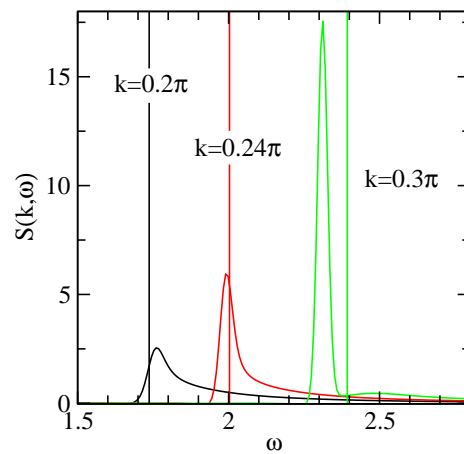


FIG. 16: $S(k, \omega)$ near $k_c \approx 0.23\pi - 0.24\pi$ for the 4th order run using the linear prediction method. The vertical line associated with each k is the two magnon lower band edge.

and a two-magnon continuum similar to that at small k . To fit the time data as accurately as possible, we assume that the two magnon band starts exactly at the expected threshold $\omega_{\text{th}} = \min_{k'} \epsilon(\pi - k'/2 + k') + \epsilon(\pi - k/2 - k')$. The relevant values of $\epsilon(k)$ used to determine ω_{th} are far from k_c and a simple exponential fit determines the magnon peak location very accurately. We also assume that the small k threshold behavior $(\omega - \omega_{\text{th}})^{1/2}$ applies. Including, in addition, the next expansion term $(\omega - \omega_{\text{th}})^{3/2}$, we utilize the fitting form (cf Eq. (12))

$$A \exp(-i\bar{\omega}t) + B \exp(-i\omega_{\text{th}}t)(b + it)^{-3/2} + C \exp(-i\omega_{\text{th}}t)(c + it)^{-5/2}. \quad (27)$$

Results from this fitting followed by Fourier transforming are shown in Fig. 17. The fits deviated from the data over the range $t = 10 - 20$ typically by a few times 10^{-5} , and the magnitude of the data points fitted to was typically near 0.1—an excellent fit, making a convincing case that the assumed asymptotic form is correct and that the results for $S(k, \omega)$ are very accurate. The peak locations from these fittings were used in the determination of the dispersion relation of Section III near k_c .

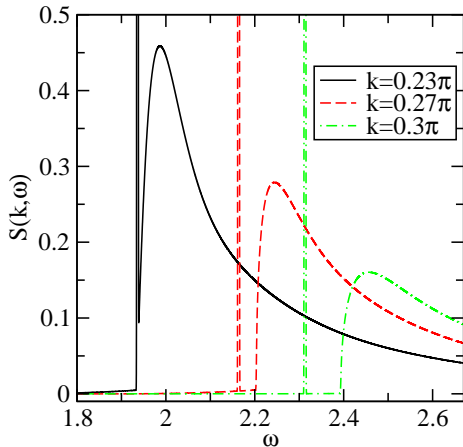


FIG. 17: $S(k, \omega)$ near $k_c \approx 0.23\pi - 0.24\pi$ for the 4th order run using fitting to the asymptotic time decay.

One can view the split-off of the single magnon peak from the two particle continuum at k_c in two different ways. First, in an approach motivated by the small k two-magnon nature of the spectrum, one can regard the splitoff as due to the formation of a sharp 2-magnon bound state for $k > k_c$.¹⁰ Second, if we imagine that k_c is “large” so that the two magnon description is inappropriate, then we can regard the single magnon peak as surviving for k near but less than k_c , but with a broadening caused by decays into two magnons. Here we will consider in more detail these two pictures.

Consider first the two-magnon bound state picture. Since the quantum numbers of the single magnon state with $S_z = 1$ and a two magnon bound state composed of a $S_z = 0$ and a $S_z = 1$ magnon are identical, we are free to regard the excitation which splits off in either way. Well above k_c the two-magnon bound state picture is clearly not very useful, since its formation would imply large magnon-magnon interactions which are not otherwise observed. The NL σ M does not have any bound states. Furthermore, in *any* Lorentz invariant theory, increasing the centre of mass momentum can never lead to bound state formation. As was discussed in Ref. 10, since the bosonic magnon excitations form a triplet, and any excitation produced from the singlet ground state by the spin operators must also be a triplet, it follows that the bound state wave-function must be antisymmetric in its spatial coordinates. In Ref. 10, it was found that the effective magnon-magnon interaction is *attractive* in the

antisymmetric channel. On the other hand, it is apparently repulsive in the symmetric channel. This is related to the BEC picture of the transition at a critical magnetic field¹³ where the Zeeman energy equals Δ .

Even in one dimension, an arbitrarily weak attraction does not produce a bound state in the antisymmetric channel (although it does produce one in the symmetric channel.) It was observed in Ref. 10 that as k is increased from zero, the momenta of the two magnons forming the bound state near the threshold $\omega_{min}(k)$, which are near $\pi + k/2$, approach the inflection points $k_{in} \approx 1.131\pi$. To study the bound state near the threshold, we can expand the dispersion relation, ϵ , near $\pi + k/2$. The momenta of the two bosons are: $\pi + k/2 \pm q$. Expanding the total kinetic energy in powers of q gives the effective kinetic energy :

$$T \approx 2\epsilon + \epsilon^{(2)}q^2 + \frac{\epsilon^{(4)}}{12}q^4 + \dots, \quad (28)$$

where ϵ and its derivatives are evaluated at $\pi + k/2$. We see that the effective mass for the centre of mass motion is given by:

$$\frac{1}{2m} = \epsilon^{(2)}(\pi + k/2). \quad (29)$$

($1/m$) vanishes at the inflection point, $k \rightarrow 2k_{in} - 2\pi \approx 0.262\pi$ and the effective kinetic energy becomes quartic. At k_{in} , the coefficient of the quartic term is $\epsilon^{(4)}/12 \approx 3.341 > 0$. For a quartic kinetic energy, an arbitrarily weak attraction leads to a bound state, in both symmetric *and* antisymmetric channel. (For the antisymmetric case this can be seen by considering a trial wave-function of $\propto x e^{-x^2/(2w^2)}$). The potential energy can be assumed to be everywhere less than a square well of depth v_0 and width a . For $w \gg a$, the potential energy is less than a quantity $\propto -v_0(a/w)^3$, while the kinetic energy is $\propto (1/w)^4$. For small v_0 , this has a negative minimum at $w \propto 1/v_0 \gg a$, proving the existence of an antisymmetric bound state with binding energy $\propto v_0^4$.) This argument implies that $k_c < 2|\pi - k_{in}| \approx .262\pi$, since for any attractive potential, as the effective mass diverges the bound state will eventually form. It is interesting to note that our DMRG estimate of $k_c \approx 0.23\pi - 0.24\pi$ is only very slightly less than $2|\pi - k_{in}|$, suggesting that the attractive interaction between magnons is weak. In addition, the splitting of the peak from the two magnon continuum varies as $(m - m_0)^2$ (where m_0 is the mass at $k = k_c$) and thus as $(k - k_c)^2$ within this bound state picture.

Now consider the second picture of the split-off, that of a magnon entering the continuum, but surviving in a broadened form near k_c . In this case one would expect for $k > k_c$ the single magnon peak and the two magnon continuum would vary independently with k and that the splitting of the peak from the two magnon continuum would be linear in $k - k_c$. In Fig. 18, we show this splitting near k_c . Indeed, the splitting appears to be linear in $k - k_c$. Below k_c , the broadening grows very

rapidly. If the splitting is quadratic in $k - k_c$, it must be so only very close to k_c .

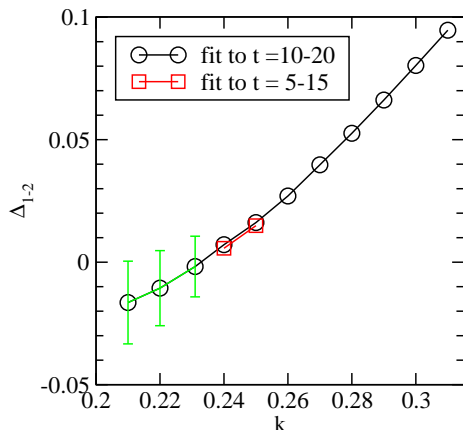


FIG. 18: Splitting between the single magnon peak and the bottom of the two magnon band near k_c determined from a fit of the time dependent DMRG data. For $\omega \geq 0.24$, the data was fit well assuming the single magnon peak was a delta function; below a better fit was obtained assuming the peaks was broadened as a Gaussian. The “error bars” indicate the width of the Gaussian.

The behavior of the splitting versus $k - k_c$ favors the second picture of the split-off. However, we cannot rule out that the two-magnon bound state picture applies very close to k_c . Note that within the two magnon bound state picture, there does not seem to be a compelling reason for more than a small fraction of the spectral weight to appear in the bound state. In fact, as shown in Fig. 11, about 50% of the spectral weight appears in the single magnon peak near $k \approx 0.25$, but the weight in the peak is rapidly falling as k is decreased.

It is also interesting to examine the line shape for k slightly less than k_c . In order to compare line shapes for different k 's, in Fig. 19 we have shifted the curves to make the two-magnon thresholds identical, and have scaled them to make them identical at the arbitrary point $\omega_{th} + 0.25$. These curves were made using the linear prediction method. The curve for $k = 0.2\pi$ shows a sharp resonance persists below but near k_c . This resonance disappears by the time k is reduced to 0.14π .

VII. CONCLUSIONS

The combination of time dependent DMRG and extrapolation of the time dependent correlation functions

has proved to be an extremely effective method for calculating spectral functions for the $S = 1$ chain. We have been able to study fine details of the spectra with much greater resolution and accuracy than with any previous method. In comparing with free boson and nonlinear sigma model predictions for features of the spectra near $k = 0$ and $k = \pi$, we find good qualitative agreement,

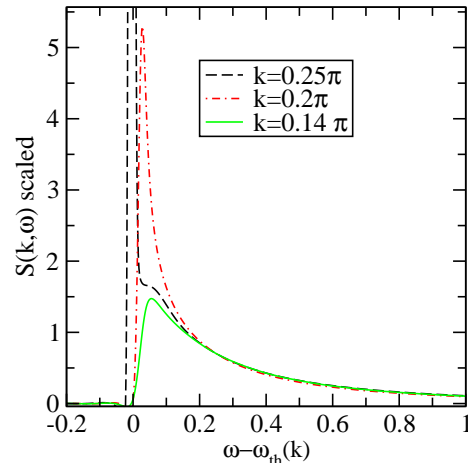


FIG. 19: $S(k, \omega)$ near and below $k_c \approx 0.23\pi - 0.24\pi$ for the 2nd order run. Each curve is shifted by the two-magnon threshold energy $2\varepsilon(k/2)$, and scaled by an arbitrary factor to make $S(k, \omega - \omega_{th} = 0.25)$ identical in each of the three curves.

but quantitative disagreements in the overall magnitude of the spectrum and in the high frequency tails. Our results near k_c where the single magnon peak enters the two magnon continuum are better described in terms of a single magnon exhibiting decay and scattering below k_c rather than viewing the single magnon peak as the formation of a two magnon bound state above k_c .

We acknowledge very helpful discussions with David Huse. We acknowledge support from the NSF under grant DMR-0605444 (SRW), from NSERC (IA), and from CIFAR (IA).

¹ S.R. White, Phys. Rev. Lett. **69**, 2863 (1992); S.R. White, Phys. Rev. B **48**, 10345 (1993). See also U. Schollwöck, Rev. Mod. Phys. **77**, 259 (2005).

² For another DMRG approach to dynamics for the $S = 1$ and $S = 1/2$ Heisenberg chains, see T. D. Kühner and S. R. White, Phys. Rev. B **60**, 335 (1999) and references

therein.

- ³ G. Vidal, Phys. Rev. Lett. **91**, 147902(2003); and quant-ph/0310089.
- ⁴ S.R. White and A. E. Feiguin, Phys. Rev. Lett. **93**, 076401 (2004).
- ⁵ A.J. Daley *et al.*, J. Stat. Mech.: Theor. Exp. P04005 (2004).
- ⁶ S.R. White and A. E. Feiguin, Phys. Rev. Lett. **93**, 076401 (2004).
- ⁷ R.G. Pereira, S.R. White, and I. Affleck, Phys. Rev. Lett. accepted.
- ⁸ E. Forest and R.D. Ruth, Physica D **43**, 105 (1990). See also I.P. Omelyan, I.M. Mryg lod, R. Folk, Comp. Phys. Comm **146**, 188 (2002).
- ⁹ See Press, et. al, Numerical Recipes, section 13.6. We perform a complex generalization of the extrapolation described there, and we control for unstable, exponentially growing modes by reflecting them into the unit circle..
- ¹⁰ S. R. White and D. A. Huse, Phys. Rev. B **48**, 3844 (1993).
- ¹¹ I. Affleck and R.A. Weston, Phys. Rev. B **45**, 4667 (1992).
- ¹² M.D.P. Horton and I. Affleck, Phys. Rev. B **60**, 11891 (1999).
- ¹³ E.S. Sorensen and I. Affleck, Phys. Rev. Lett. **71**, 1633 (1993).